Two coupled double quantum-dot systems as a working substance for heat machines

Jefferson Luan Diniz de Oliveira
Departamento de Física, Universidade Federal da Paraíba, Caixa Postal 5008, 58059-970 João Pessoa, PB, Brazil

Moisés Rojas and Cleverson Filgueiras
Departamento de Física, Universidade Federal de Lavras, Caixa Postal 3037, 37200-900 Lavras-MG, Brazil

(Received 1 February 2021; revised 5 May 2021; accepted 1 July 2021; published 30 July 2021)

This paper presents a conceptual design for quantum heat machines using a pair of coupled double quantum dots (DQDs), each DQD with an excess electron to interact, as an working substance. We define a compression ratio as the ratio between the Coulomb couplings which describes the interaction between the electrons during the isochoric processes of the quantum Otto cycle and then we analyze the arising of different regimes of operations of our thermal machine. We also show that we may change the operation mode of an Otto engine when considering the effects due to the *quantum tunneling* of a single electron between each individual DQD.

DOI: 10.1103/PhysRevE.104.014149

I. INTRODUCTION

Despite thermodynamics and quantum mechanics seems to be, at first sight, contradictory theories, early in 1959 Scovil and Schulz-DuBois [1] demonstrated through an equivalence between a three-level maser and a Carnot heat engine that it is possible to conciliate them. Since them, there are plenty of proposals for quantum heat engines and how the thermodynamic processes, or even the laws of thermodynamics [2], can be defined in the microscopic world of quantum mechanics [3].

Beyond the quasiequilibrium point of view of thermal machines, the pioneer work of F. L. Curzon and B. Ahlborn [4] started the search for *endoreversible machines*, which takes into account the time it takes for the thermodynamic processes to occur. This enables the search for the maximum power output of a heat engine, which is the most important physical quantity for practical purposes [5,6]. In the realm of quantum mechanics, the time is not a physical observable, but we highlight here the work of R. Alicki [7] that formally defines the thermodynamic concepts for the quantum open systems in the Markovian regime that consider a finite period for each thermodynamic cycle to be started and finished. Over the past few decades many proposals has been settle for quantum heat engines with different working substances, such as trapped ions [8–11]; quantum oscillators [12–14]; Heisenberg XX, XY, XXX, XXZ, or XYZ spin models with Dzyaloshinskii-Moriya interaction [15–19]; quantum dots [20,21]; etc.

On the other hand, there is a great interest in the study of quantum dots in different aspects, like its optical and electronic properties in the production for displays [22,23] or photovoltaic devices [24,25] or even in the context of quantum information processing [26–28]. A quantum dot is a semiconductor particle and it is sometimes called an "*artificial atom*" because of its similarities with a real one. The differences between them are their size (at least three orders of magnitude greater than an atom), their shape and the strength of the confining potential. Double quantum dots (DQDs) are, as the name suggests, two quantum dots coupled in series [29,30]. Then, it is straightforward to understand why they are sometimes called "*artificial molecules*." The quantum dynamics and entanglement of two electrons inside the coupled DQDs were investigated in Refs. [31,32] and the aspects related to the quantum correlations and to the decoherence were addressed in Refs. [33,34]. The Ref. [35] gives us a picture of a pair of coupled DQDs, showing the behavior of thermal entanglement and the correlated coherence behaves in this system as we adjust some parameters. Following this scenario, in this contribution, we implement the thermodynamic concepts of a quantum heat engine for this very same system. Each DQD is filled with a single electron that can tunnel (or not) between each individual island. This is possible due to quantum tunneling and Coulomb blockade effects [36,37], which are observed in very small devices, as in our case: We consider quantum dots separated by tunnel junctions that act as an insulating barrier. The quantum tunneling has a central role in our findings since it shows to be a parameter that may changes the operational mode of a heat machine we are proposing. Although the paradigm in this field is the investigation of finite time cycles in open quantum systems, at this stage we focus in the quasistatic process so that the system will be described at the end of an isochoric strokes by a Gibbs state, which means that it is in a thermal equilibrium with a heat bath. Nevertheless, we will present important insights which we believe are going to survive in this context but need to be clarified. Here it is shown that by controlling the effects due to a quantum tunneling of a single electron between each individual DQD, the performance of both the engine and the refrigerator can be improved and the operation mode of the machine can be yet altered, yielding the possibility of work extraction even for the case where the Coulomb coupling is unaltered.

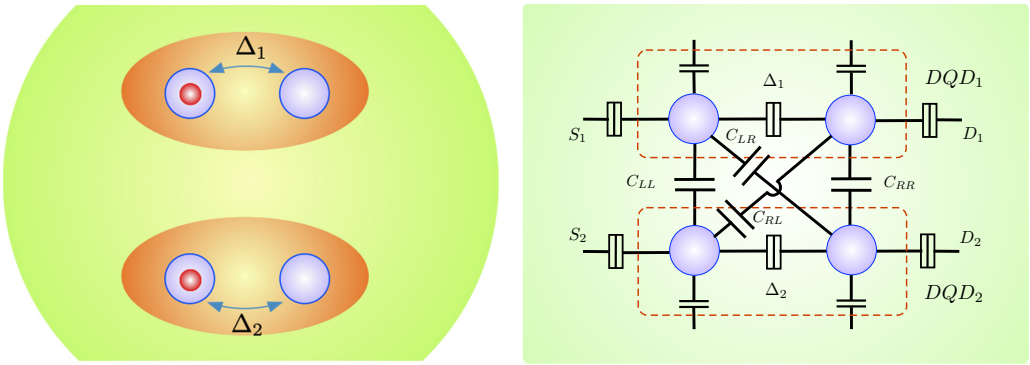

FIG. 1. The left picture shows a schematic representation of the physical model with two coupled DQDs. The purple spheres represent the quantum dots, the electrons are represented by the smaller red spheres inside the quantum dots and $\Delta_{1,2}$ stands for the tunneling coupling of the $DQD_{1,2}$. The right picture is the equivalent circuit diagram of the device. Tunnel couplings are represented by two bars as in Δ_1 and Δ_2, $S_{1,2}$ and $D_{1,2}$ are, respectively, the source and drain of the $DQD_{1,2}$, and the capacitors C_{LL}, C_{RR}, C_{LR}, and C_{RL} connect the DQDs.

This paper is organized as follows: In Sec. II we present a general overview of the system and how we are going to accost it. In Sec. III we discuss the processes involving the quantum Otto cycle and then calculate both the total work done and the engine efficiency. In Sec. IV we discuss the results and analyze minutely the emergence of different regions of regime for the quantum heat engine. In Sec. V we present the concluding remarks that summarize our results.

II. A PAIR OF DOUBLE QUANTUM DOTS AS AN WORKING SUBSTANCE

The proposed quantum system as an working substance for quantum heat engines can be described by the two-qubit device that is fabricated in a standard AlGaAs/GaAs heterostructure with two-dimensional electron gas (2DEG) by using electron beam lithography. The device consists of a series of Schottky gates[1] and the electron configurations in both DQDs are controlled by tuning the voltages applied on the gates (see Fig. 1). On the other hand, the two double quantum dots are capacitively coupled, this capacitance model describing the Coulomb interactions between the two DQDs [29,38,39]. This capacitance coupling is controlled by the capacitors C_{LL}, C_{RR}, C_{LR}, and C_{RL}, where no transition for the electron to leave the DQD_1 into DQD_2 is allowed and vice versa. The tunnel junctions placed after the source $S_{1,2}$ and before the drain $D_{1,2}$ are adjusted in such a way to make the system in the Coulomb blockade regime, enabling a single electron to be confined in each DQD. The charge of the electron in each DQD build up the qubits, which are described by the two possible states for the location of each electron, the left dot ($|L\rangle$) and the right dot ($|R\rangle$), where the electron can tunnel from left to right and from right to left. The Hamiltonian of such a system is given by

$$H = \Delta_1\sigma_1^x + \Delta_2\sigma_2^x + V\left(\sigma_1^z \otimes \sigma_2^z\right), \tag{1}$$

where Δ_1 and Δ_2 are the strength of the tunneling coupling between each pair of quantum dots, V is the interaction Coulomb coupling between the excess electrons, and $\sigma_{1(2)}^{x,y,z}$ are the Pauli matrices. The tunneling coupling parameters Δ_1 and Δ_2 are controlled by the gate voltages (Schottky gates) and the electrostatic coupling V between the double quantum dots is controlled by the gates voltage sources S_1 (S_2) through the capacitors connecting both DQDs. A more general version of the Hamiltonian of this system takes into account an extra term for the energy differences between the uncoupled charged states $|L\rangle$ and $|R\rangle$, but the difficulties behind solving its equations are not in the scope of our aim in this paper. This way, we consider the simplest case where all of our quantum dots have the same energy available for the electron to occupy.

Solving the eigenvalue equations for the Hamiltonian (1), we obtain the following eigenstates (see Ref. [35]):

$$\begin{aligned}
|\psi_1\rangle &= \alpha_-[A_-(-|LL\rangle + |RR\rangle) + n_-(|LR\rangle - |RL\rangle)],\\
|\psi_2\rangle &= \alpha_-[n_-(-|LL\rangle + |RR\rangle) + A_-(-|LR\rangle + |RL\rangle)],\\
|\psi_3\rangle &= \alpha_+[A_+(|LL\rangle + |RR\rangle) + n_+(|LR\rangle + |RL\rangle)],\\
|\psi_4\rangle &= \alpha_+[n_+(|LL\rangle + |RR\rangle) - A_+(|LR\rangle + |RL\rangle)],
\end{aligned} \tag{2}$$

where $\alpha_\pm = \frac{1}{\sqrt{2}\sqrt{(n_\pm)^2+A_\pm^2}}$, $A_\pm = V + \sqrt{(n_\pm)^2+V^2}$, and $n_\pm = \Delta_1 \pm \Delta_2$, with the following eigenenergies:

$$E_1 = -\sqrt{(n_-)^2+V^2}, \tag{3}$$

$$E_2 = -\sqrt{(n_+)^2+V^2}, \tag{4}$$

$$E_3 = \sqrt{(n_-)^2+V^2}, \tag{5}$$

$$E_4 = \sqrt{(n_+)^2+V^2}. \tag{6}$$

An important result that we will later need is how the eigenenergies change as either the Coulomb coupling or one of the tunneling parameters increases (it does not matter which of them we take since the Hamiltonian is symmetric as we change $\Delta_1 \leftrightarrow \Delta_2$). From the Fig. 2 we see that the energy levels are compressed pairwise and, at the same time, the ground and the first excited state are separated from the second and

[1]The Schottky gates are not illustrated in Fig. 1 due to the high number of gates usually implemented experimentally.

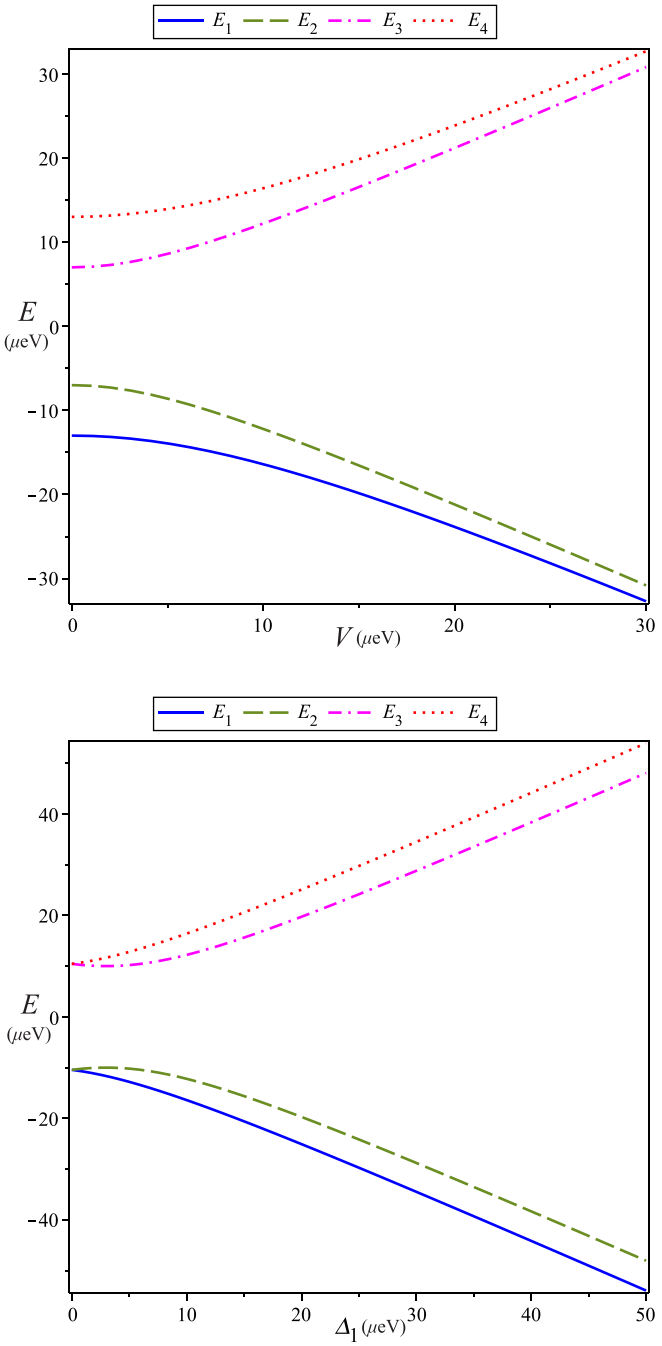

FIG. 2. In (a), it is depicted the energy levels in terms of the interaction coupling V between the two DQDs for the same fixed tunneling parameters $\Delta_1 = 10\ \mu$eV and $\Delta_2 = 3\ \mu$eV. In (b), we have the plot of the energy levels against the tunneling parameter Δ_1 for fixed $\Delta_2 = 3\ \mu$eV and $V = 10\ \mu$eV. Notice that there is a squeezing of the energy gaps as we either increase the interaction coupling or decrease the tunneling parameter.

third excited states as the interaction coupling is raised. On the other hand, the energy levels are pairwise detached. As we increase the tunneling parameter, they are shifted apart from each other more rapidly than the energy-level separation observed inside each pair separately. Thus the energy scale variation is not uniform. This way, as a first approach, we will

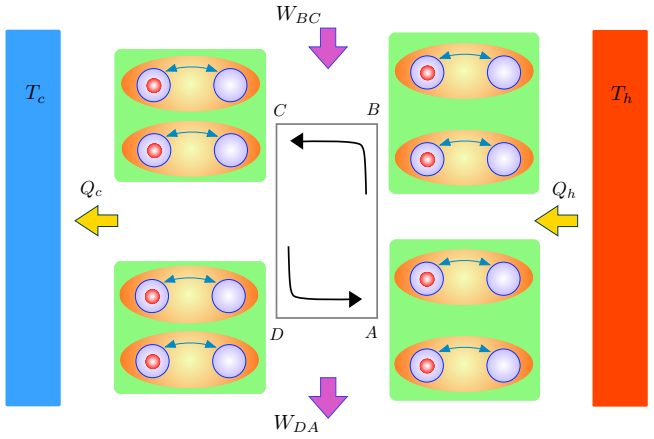

FIG. 3. A schematic representation of an Otto engine using a pair of coupled DQDs as a working substance: The incoming heat from the hot bath, Q_h, is transformed into extracted work. The engine cycle consists of two adiabatic strokes ($B \to C$ and $D \to A$) where it is decoupled from the thermal baths, and two isochoric strokes ($A \to B$ and $C \to D$) where the engine is coupled to two thermal baths at temperatures T_h and T_c, with $T_h > T_c$.

approximate our system by a two-level one with energies E_1 and E_2.

Despite the values of the tunneling parameters, Δ_1 and Δ_2, are mostly predetermined in the fabrication of the device, we still can modify them experimentally [29].

Here we refer the system as in a Gibbs state when it is in a thermal equilibrium with a heat bath, which means that its density matrix is given by $\rho(T) = \frac{\exp(-\beta H)}{Z}$, where Z is the partition function, $\beta = \frac{1}{kT}$, k is the Boltzmann constant, and T is the temperature of the heat bath.

III. THE QUANTUM OTTO ENGINE CYCLE

In this section we describe the quasistatic quantum Otto engine cycle, which operates in four strokes: two quantum isochoric processes and two quantum adiabatic processes (see Fig. 3).

The cycle starts with a quantum isochoric process ($A \to B$): The working substance, with interaction coupling V_h and tunneling parameters Δ_1^h and Δ_2^h, is put in contact with the hot reservoir at temperature T_h until they reach a thermal equilibrium and a total heat $Q_h > 0$ is transferred to the system at the end of the process. The parameters V, Δ_1, and Δ_2 that regulate the eigenenergies are controlled externally, what makes this process easier to realize in an experiment. At the end of the process we will have, for the energy eigenstate basis $\{|\psi_n\rangle\}$, the following density matrix:

$$\rho_h = \exp(-H_h/kT_h)/Z_h = \sum_n p_n^h |\psi_n\rangle \langle\psi_n|, \tag{7}$$

with

$$H_h = \sum_n E_n^h |\psi_n\rangle \langle\psi_n|, \tag{8}$$

$$p_n^h = \exp\big(-E_n^h/kT_h\big)/Z_h, \tag{9}$$

$$Z_h = \sum_n \exp\big(-E_n^h/kT_h\big), \tag{10}$$

where Z_h is the partition function, p_n^h is the occupation probabilities of each eigenstate, and H_h is the Hamiltonian when the system is in contact with the hot heat bath.

Next, we have a quantum adiabatic expansion ($B \to C$). In this process no heat is exchanged between the system and the environment. The working substance is totally isolated from the environment and therefore, the Eq. (9) is no longer valid during the process because there is no thermal equilibrium with it. Thus we can increase the interaction coupling from V_h to $V_c > V_h$ by adjusting the charge state through the gates voltage sources S_1 (S_2) in the capacitors mentioned in Fig. 1 and still keep the occupation probabilities p_n^h constant until the end of the process. Moreover, in parallel to this, the tunneling parameters may be tuned from $\Delta_1^h(\Delta_2^h)$ to $\Delta_1^c(\Delta_2^c)$ by controlling the gate voltages in each DQD. Thereby the energies increases from E_n^h to E_n^c, so the Hamiltonian will be given by $H_c = \sum_n E_n^c \left|\psi_n\right\rangle \left\langle\psi_n\right|$ and some work $W_{BC} > 0$ is extracted from the system.

In the next stroke we have another quantum isochoric process ($C \to D$). We put the working substance in contact with the cold reservoir at temperature T_c, waiting enough time for the thermalization to occur. A total heat $Q_c < 0$ is transferred to the cold reservoir at the end of the process and, since heat is exchanged, the occupation probabilities change from $p_n^h = \exp(-E_n^h/kT_h)/Z_h$ to $p_n^c = \exp(-E_n^c/kT_c)/Z_c$, with $Z_c = \sum_n \exp(-E_n^c/kT_c)$. The density matrix will be given by $\rho_c = \exp(-H_c/kT_c)/Z_c = \sum_n p_n^c \left|\psi_n\right\rangle \left\langle\psi_n\right|$ and we keep the energies E_n^c fixed.

Finally, we close the cycle with a quantum adiabatic compression ($D \to A$). At this point, we adjust the voltages in the capacitors again, causing the interaction coupling to change from V_c to V_h. Apart from that, the tunneling parameters may be tuned from $\Delta_1^c(\Delta_2^c)$ to $\Delta_1^h(\Delta_2^h)$ and, consequently, the energies from E_n^c to E_n^h. The Hamiltonian of the system in the end of the process is then $H_h = \sum_n E_n^h \left|\psi_n\right\rangle \left\langle\psi_n\right|$, the occupation probabilities p_n^c are kept unchanged and some work $W_{DA} < 0$ is done on the working substance.

As stated in Ref. [35] we can say that when the working substance is in contact with the hot reservoir, it is in a weakly correlated state and, as we increase the interaction coupling and decrease the temperature, the system starts to be more correlated.

The quantum version of the first law of thermodynamics in the quasistatic limit allow us to calculate the total heat exchanged during the isochoric processes [3], that is,

$$Q_h = \sum_n E_n^h \left(p_n^h - p_n^c\right), \tag{11}$$

and

$$Q_c = \sum_n E_n^c \left(p_n^c - p_n^h\right), \tag{12}$$

where $Q > 0$ ($Q < 0$) means that heat is absorbed (released) from (to) the heat reservoirs, respectively. Therefore, the total work W produced by the heat engine in the adiabatics is, by energy conservation, the excess heat

$$W = Q_h + Q_c = \sum_n \left(E_n^h - E_n^c\right)\left(p_n^h - p_n^c\right). \tag{13}$$

With that in hands, we can finally have the efficiency of our heat engine, which is calculated by $\eta \equiv W/Q_h$.

The description of the refrigerator cycle is totally analogous to the processes of the heat engine discussed early, except for the direction of operation of the cycle, which is reversed. This means that we will have a heat released $Q_c > 0$ from the cold heat bath and absorbed $Q_h < 0$ by the hot heat bath to the working substance and, consequently, it will be necessary an external work $W = Q_h + Q_c < 0$ for the cycle to operate. The coefficient of performance (COP) ε measures the efficiency of the refrigerator, which is defined as the modulus of the ratio of heat released from the cold heat bath and the total work done in the cycle, that is, $\varepsilon \equiv Q_c/W$.

With those definitions in hand, in the next section we investigate in detail the work, the efficiency η and the COP ε. Although this work is theoretical, a possible implementation of the thermal machine with double quantum dots is to consider the recent concept of particle-exchange heat engines, which uses energy filtering to control a thermally driven particle flow between two heat reservoirs. As they do not require moving parts and can be realized in solid-state materials, they are suitable for low-power applications and miniaturization [20].

IV. RESULTS AND DISCUSSION

In order to plot the next graphics, we restrict ourselves to the case where the tunneling parameters Δ_1 and Δ_2 are the same for the whole cycle and we will no longer worry about the upper index. This way we define a compression ratio r as the ratio between the maximum and the minimum interaction coupling values in the cycle, $r = V_c/V_h$. As we have previously discussed, the Coulomb interaction is modified by the controlling voltages in the capacitors. Since a quantum dot is typically regarded as a 0D system, for which the actual spatial dependence is not considered, the parameter r cannot be seen due to the changing of the volume of the system. The energy-level spacing of the system is the quantity that is being either compressed or stretched.

In the Fig. 4 the heat exchanged Q_h (Q_c) with the hot (cold) reservoir, the work done W, the efficiency η and the Carnot efficiency η_c are given in terms of the compression ratio r, where we have set[2] $\Delta_1 = 10\ \mu$eV, $\Delta_2 = 3\ \mu$eV and $T_h = 2\ \mu$eV, $T_c = 1\ \mu$eV (we normalize the Boltzmann constant $k = 1$ in this whole paper). It is clear from the Fig. 4 that we need $r > 1$ ($V_c > V_h$) to achieve positive work, which is reasonable because in this regime the energy gaps are squeezed (see Fig. 2) when the system is in contact with the cold reservoir and they are expanded when the system is in contact with the hot reservoir [40]. Note that we can not increase the compression ratio r indefinitely since the positive work condition is lost. As we increase the value of r, it comes to a point where there is no heat transfer even when the system

[2]The choice of the values for the tunneling parameters are not random: For either $\Delta_1 \approx \Delta_2$ or $\Delta_2 \gg \Delta_1$ (or even $\Delta_1 \gg \Delta_2$) the work achieved is minimum, see Appendix A. See also Appendix B for an explanation on how these values for the reservoirs temperatures enables the two-level approximation.

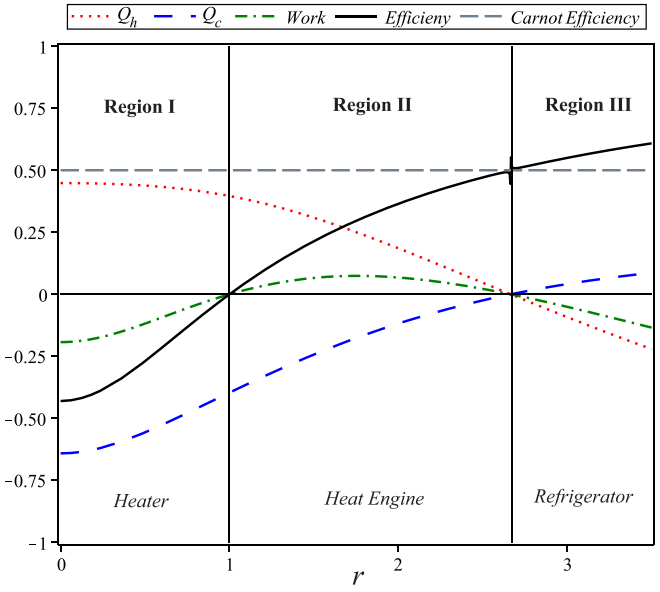

FIG. 4. As illustrated, we have the heat exchanges of the working substance with the hot and cold reservoirs (Q_h and Q_c, respectively), the work W done, the efficiency η and the Carnot efficiency η_C of the heat engine against the compression ratio r. Heat transfer between the hot and cold reservoir. A sign inversion on the flow of the heat happens as we increase the compression ratio r. For this plot, we have chosen the values $V_h = 10\ \mu$eV, $\Delta_1 = 10\ \mu$eV, $\Delta_2 = 3\ \mu$eV, $T_h = 2\ \mu$eV, and $T_c = 1\ \mu$eV. The values of Q_h, Q_c, and W are given in units of μeV.

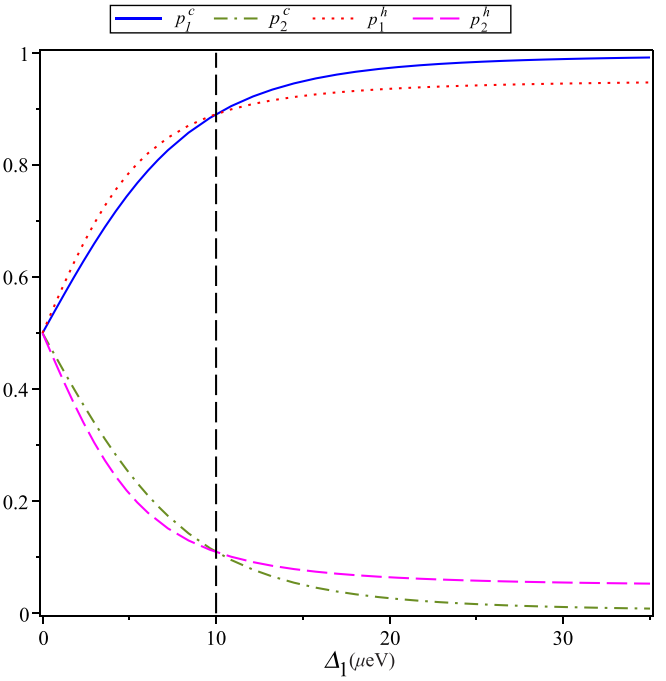

FIG. 5. The occupation probabilities curves for the ground and first excited state in the two situations are shown, when the system is in contact with the hot heat bath and the cold heat bath. The probabilities curves for higher excited states are omitted because their values are close to zero for these values that we take, to know, $V_h = 10\ \mu$eV, $\Delta_2 = 3\ \mu$eV, $T_h = 2\ \mu$eV, $T_c = 1\ \mu$eV, and $r = 2.67$, which is approximately the value of the compression ratio where the inversion of the heat fluxes occurs.

is in contact with the hot and the cold reservoir. Furthermore, after this point, the signs of the heats exchanged are inverted and the system starts to withdraw heat from the cold reservoir and transfer heat into the hot reservoir. In other words, the system starts behaving as a refrigerator at cost of some work.

To summarize, we can see the appearing of three different regions of operation for the heat engine. In the region I the engine requires a negative work $W < 0$ to extract heat from the hot to the cold reservoir, i.e, the machine operates as a heater. In the region II we have a positive work, $W > 0$, which means that the it acts as a heat engine producing useful work. Finally, the region III correspond to a refrigerator as we have already discussed early, because we have an inversion on the flow of the heat for some negative work $W < 0$. These results show that we can pass through the different regimes by simply increasing a single parameter, the interaction coupling V_c (which causes the change in r). Another way to interpret this inversion of heat fluxes is by observing that as we increase the value of the Coulomb coupling the system gets more and more strongly correlated so that there is a value of concurrence that is critical where the signs of the transferred heats are exchanged [35].

Notice that the two points where the dash-dotted green curve of the work done intersects the r axis in the Fig. 4 have different meanings: The first one has to do with the equality in modulus of the heat Q_h and Q_c [see Eq. (13)], i.e., all of the heat absorbed from the hot reservoir is released to the cold reservoir, and the second one has to do with the totally interruption of the heat transferred to both reservoirs. This interruption can be explained by means of the occupation probabilities $p_n^h = \exp(-E_n^h/kT_h)/Z_h$ and $p_n^c = \exp(-E_n^c/kT_c)/Z_c$, where we can see in the Fig. 5 that there is a point where the occupation probabilities curves for the hot and cold heat baths intersects, which means that in this regime there is no change on the occupation probabilities of the system when it passes from the hot heat bath to the cold heat bath, what causes the interruption of the heat flux.

After zooming the Fig. 4, we can extract an additional information about the "*point*" that causes the divergence on the efficiency plot. First, as we can see from the Fig. 6, there is no such a thing as a point that simultaneously invert the signs of the heat exchanged Q_h and Q_c. Before the efficiency explodes, the work tends to zero, and so the efficiency, where over again we have the heat pump regime. After an almost infinitesimal increase on r, there is an explosive increase on efficiency due to the interruption on the heat flow Q_h (remember that $\eta = W/Q_h$). After this point, the system does not immediately starts behaving as a refrigerator, we have a tiny region where the machine consumes work and exhaust heat for both reservoirs (we use here the notations of the Ref. [41] for the two different kinds of heat pump, to know, *heater I* for the usual heater and *heater II* for the machine that heats both reservoirs, see also Ref. [42]). Only after that, we will have a positive heat flow from the cold reservoir to the system turning the machine into a refrigerator.

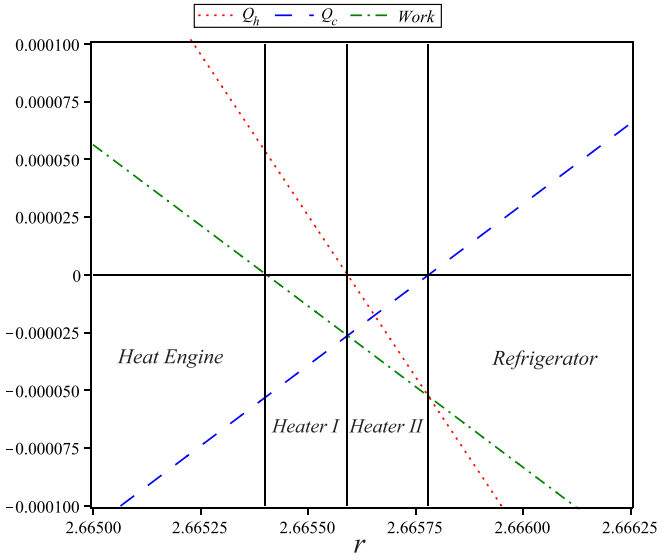

FIG. 6. As illustrated, we have the work done W (dash-dotted green), the heat absorbed Q_h (dotted red) and released Q_c (loosely dashed blue) against the compression ratio r: The observed behavior remind us something like a phase transition. We keep the same values, as usual, $V_h = 10\ \mu$eV, $\Delta_1 = 10\ \mu$eV, $\Delta_2 = 3\ \mu$eV, $T_h = 2\ \mu$eV, and $T_c = 1\ \mu$eV. The values of Q_h, Q_c, and W are given in units of μeV.

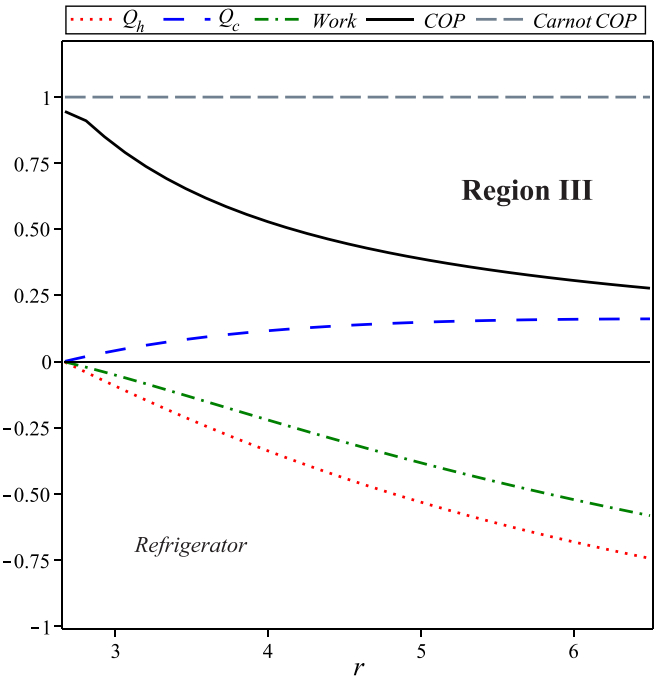

FIG. 7. As illustrated, we have the heat exchanges of the working substance with the hot and cold reservoirs (Q_h and Q_c, respectively), the work done and the COP ε of the refrigerator against the compression ratio r. To plot this graph we have chosen the values $V_h = 10\ \mu$eV, $\Delta_1 = 10\ \mu$eV, $\Delta_2 = 3\ \mu$eV, $T_h = 2\ \mu$eV, and $T_c = 1\ \mu$eV. The values of Q_h, Q_c, and W are given in units of μeV.

A. The refrigerator regime

After the point where the heat fluxes are inverted that we discussed previously, the machine starts behaving as a refrigerator, thus we can evaluate the COP for it. Similarly as before, we make plots containing all the important information about the refrigerator at this stage. This is carried out in Fig. 7 where we put the heat transferred to the hot and to the cold reservoirs, the work done, the COP of a Carnot refrigerator and the COP against the compression ratio r. It is important to mention that the definition of COP is only valid in the region III (see Fig. 6). Note that the COP is a monotonically decreasing function of the compression ratio.

B. The influence of the quantum tunnelling

Early we have restricted ourselves to the case where there is no change on the tunneling parameters Δ_1 and Δ_2. Although we have found some interesting features for the heat engine, still nothing too different from the classical one was observed. As it is well known, quantum tunneling is not predicted by the laws of classical mechanics: For a particle to surpass a potential barrier it is required potential energy. In the light of recent papers, in particular the Klimovsky work [43], we can extract some unexpected features of our machine if we consider the quantum tunneling. For instance, we observe a regime where work can be extracted for unchanged Coulomb coupling, which we considered to define the compression ratio. This can be achieved by varying some gate voltages that control the tunneling parameters of the DQDs.

The classical Otto engine assumes the efficiency $\eta_O = 1 - \frac{1}{r^{\gamma-1}}$, $\gamma = C_p/C_v$ being the specific heat ratio and r the compression ratio. Note that for $r = 1$ the efficiency goes to zero and if $r < 1$ the efficiency becomes negative corresponding to the heater regime. This is exactly what happens if we keep $\Delta_1^c = \Delta_1^h$ and $\Delta_2^c = \Delta_2^h$, which is depicted in the solid blue curves of Fig. 8, thereat we will refer this particular case as the *classical case*. At this point we can abandon the constraint we made before and consider $\Delta_1^h \neq \Delta_1^c$ and $\Delta_2^h \neq \Delta_2^c$, so that new parameters $\delta_1 = \Delta_1^c/\Delta_1^h$ and $\delta_2 = \Delta_2^c/\Delta_2^h$ can be defined. The full description of the operation modes of the engine is no longer described by a single compression ratio r, but by the set of parameters $\{r, \delta_1, \delta_2\}$. In the Fig. 8 we plot the efficiency normalized to the Carnot efficiency $\eta_N = \eta/\eta_c$ in terms of r for some different values of the quantities δ_1 and δ_2. We can observe a shift of the curve to the left (right) when we have $\delta_{1(2)} < 1$ ($\delta_{1(2)} > 1$) individually or we can have a stretching (squeezing) for the left and right if we have $\delta_1 > 1$ and $\delta_2 < 1$ ($\delta_1 < 1$ and $\delta_2 > 1$) simultaneously, where $\delta_{1(2)}$ stands for "δ_1 or δ_2."

In the Fig. 8(a), specifically in the dashed red curve corresponding to $\delta_1 = 1$ and $\delta_2 < 1$, it is observed an enhancement in the efficiency in comparison to the case where the tunneling parameters are kept fixed throughout the cycle. As a consequence, no heat pump regime appears, which means that the heater was changed to a highly efficient engine and we now have a positive efficiency even for unchanged Coulomb coupling, for which $r \equiv 1$. Also, the point of inversion from heat engine to refrigerator is shifted to a lower value of r. On the other hand, when $\delta_{1(2)} > 1$ (dash-dotted green curve), we have a larger region for the operation of the heat pump and the point of inversion from heat engine to refrigerator is also shifted, but to a higher value of r instead. This means

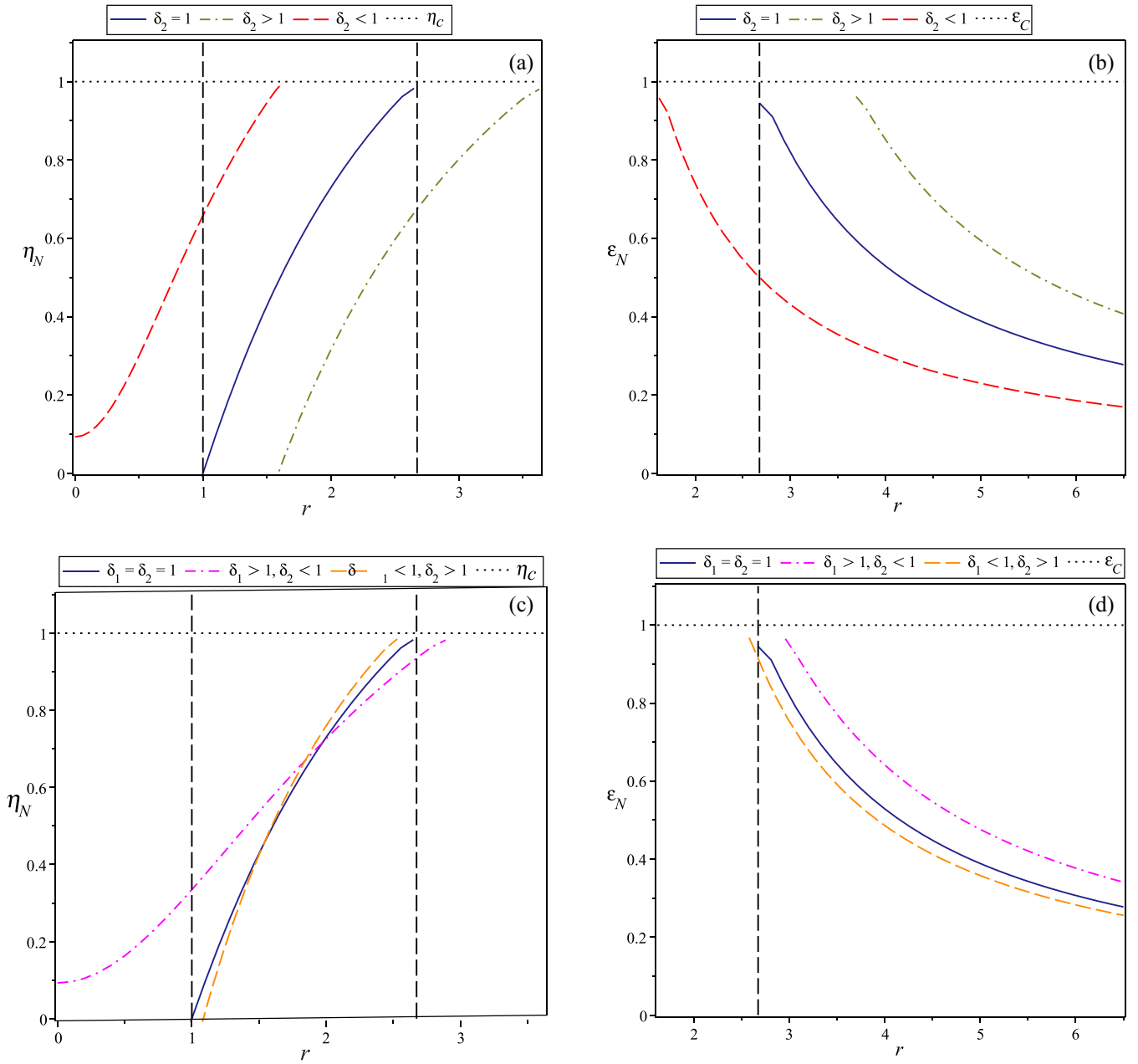

FIG. 8. In (a), it is depicted the normalized efficiency η_N and in (b), it is shown the normalized COP ε_N curve. It is considered in both of them $\delta_1 = 1$: the classical case ($\delta_2 = 1$, solid blue), the $\delta_2 > 1$ case (with $\Delta_2^c = 4\ \mu$eV, dash-dotted green), and the $\delta_2 < 1$ case (with $\Delta_2^c = 2\ \mu$eV, dashed red). In (c) and in (d), we have the normalized efficiency η_N and the normalized COP ε_N, respectively: the classical case ($\delta_1 = \delta_2 = 1$) in solid blue, the stretched dash-dotted magenta curve for $\delta_1 > 1$ and $\delta_2 < 1$ (with $\Delta_1^c = 18\ \mu$eV and $\Delta_2^c = 2\ \mu$eV) and the squeezed dashed orange curve for $\delta_1 < 1$ and $\delta_2 > 1$ (with $\Delta_1^c = 7\ \mu$eV and $\Delta_2^c = 4\ \mu$eV). For all the plots we have set $V_h = 10\ \mu$eV, $\Delta_1^h = 10\ \mu$eV, $\Delta_2^h = 3\ \mu$eV, $T_h = 2\ \mu$eV, and $T_c = 1\ \mu$eV.

that the efficiency is reduced but the region which describes the refrigerator now is valid for highly efficient engine. In Fig. 8(b), the normalized COP $\varepsilon_N = \varepsilon/\varepsilon_C$, with ε_C being the Carnot COP, is plotted for the same set of parameters values, which reinforces the results previously discussed for the efficiency η. Moreover, we observe that the refrigerator presents a better performance for higher values of r (see the dash-dotted green curve). In the Fig. 8(c), we can observe a special case for which the efficiency can be enhanced bellow some value of r while it can be diminished above it. This means that the heater is turned into an engine (not to efficient) and the refrigerator is changed to a highly efficient engine (see the dash-dotted magenta curve). The Fig. 8(d), which stands for the normalized COP $\varepsilon_N = \varepsilon/\varepsilon_C$ completes the analyzes and it shows that a refrigerator can have an improvement in its performance as well (see the dash-dotted magenta curve).

For almost all of the previous plots, we analyze the compression ratio r increasing up to 6 times, but experimental data [38] shows a variation for interaction coupling V up to almost 3 times at least (the change was from 25 to 75 μeV). This way, the previous discussions of the Fig. 8 becomes more relevant since we have, in some cases, a shift for the curve

to the left, where the compression ratio is lower, supporting the experimental possibility for the realization of all operation modes.

During this whole paper we focus only in the two-level approach, but what happens when we have higher temperatures? If we increase the temperatures of the reservoirs the most excited states in the system becomes relevant (see Appendix B). In this case, there is no inversion for the heat exchanged with the reservoirs as we can see in Fig. 9(a). The machine will never turns into a refrigerator, which sustain our explanation from the Fig. 5 where the inversion of the flow of the heat occurs because of the inversion on the occupation probabilities. Figure 9(b) shows that the machine presents very unusual properties even without varying the tunneling parameters, although no work can be done for $r \equiv 1$. In the region $r < 1$ the machine behaves as a heat engine producing useful work and for $r > 1$ the machine will be a heat pump.

Some disadvantages of our model includes a requirement of approximating our system by a two-level one for most part of our results and we consider the system completely isolated during the adiabatic processes. It is important to note that the irreversibility of the isochoric processes does not affect the efficiency of the Otto cycle. Our aim for future researches involves considering the finite time cycles, covering the problem in the open quantum systems context [5,40].

V. CONCLUSIONS

In conclusion, in this paper, we addressed a theoretical proposal for a quantum heat machine with two sets of coupled DQDs interacting via Coulomb interaction of excess electrons inside each DQD, which in turn acts as our charged qubits. We discussed the appearing of different regions of operation for our machine: the heat pump, the heat engine and the refrigerator. These operation modes can be switched by adjusting the value of the interaction coupling. We also discussed the reason why these transitions occur and what is truly happening with the machine in the null work points.

Furthermore, we do not just calculate the work done and the efficiency of the heat engine, but also the COP of the refrigerator. In addition, we gave a description on how we can escape the results expected for a classical machine. These findings rely in the effects due to variations of the parameters that control the quantum tunneling of a single electron between each individual DQD. We have observed that the performance of both the engine and the refrigerator can be modified due to the manipulation of this well known quantum phenomenon. Also, it allows the modification of the operation mode of the machine: Either a heater or a refrigerator can be switched to a highly efficient engine in some cases. We have observed the possibility of work extraction even for the case where the Coulomb coupling is kept constant. Our results follows the spirit of those found in Ref. [43], where the possibility of the modification of the operation mode of a quantum heat machine was observed as a consequence of a nonhomogeneous energy scaling.

In summary, the present work brings a new example to increment the set of already known quantum heat engines with very promising devices as the working substance, which are the DQDs, also bringing the recipe for the total manipulation of the operation modes. Thereat, the main complications still lies in the coupling with the heat baths and, thinking ahead, how the time can plays a role on this engine, but we leave these questions opened to be explored in future works.

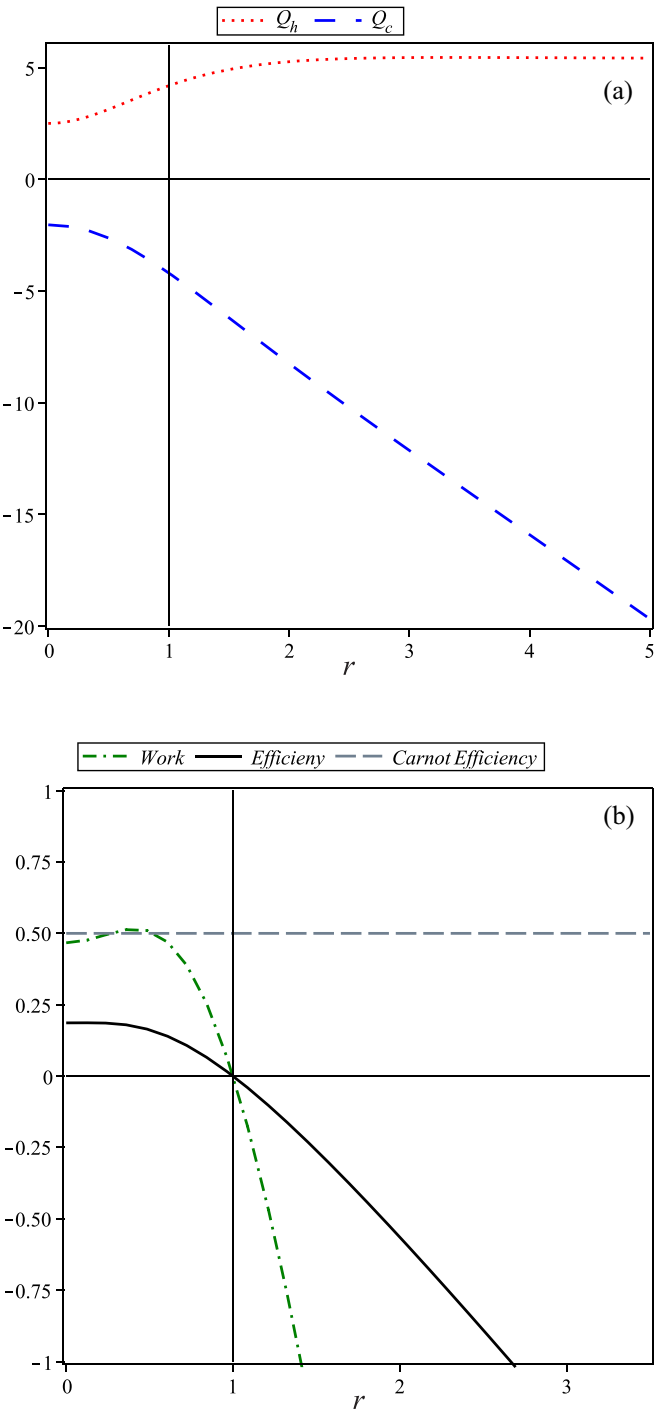

FIG. 9. In (a) we have the heat exchanged with the hot (dotted red) and cold (loosely dashed blue) reservoirs and in (b) it is depicted the work done (dash-dotted green) and the efficiency (solid black) against the compression ratio r. We have fixed $V_h = 10\ \mu$eV, $\Delta_1^h = 10\ \mu$eV, $\Delta_2^h = 3\ \mu$eV, $T_h = 20\ \mu$eV, and $T_c = 10\ \mu$eV. The values of Q_h, Q_c, and W are given in units of μeV.

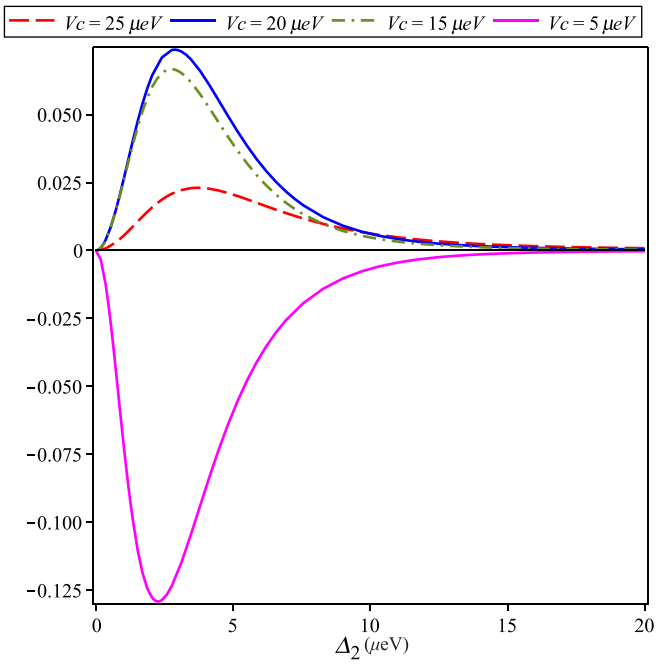

FIG. 10. The work done against the tunneling parameter Δ_2 for different values of V_c and fixed values: $V_h = 10\ \mu$eV and $\Delta_1 = 10\ \mu$eV. We have $V_c = 5\ \mu$eV [solid magenta (lower) curve], $V_c = 15\ \mu$eV (dash-dotted green curve), $V_c = 20\ \mu$eV [solid blue (upper) curve] and $V_c = 25\ \mu$eV (dashed red curve). The case $V_c = 10\ \mu$eV is not plotted, but it corresponds to a null work.

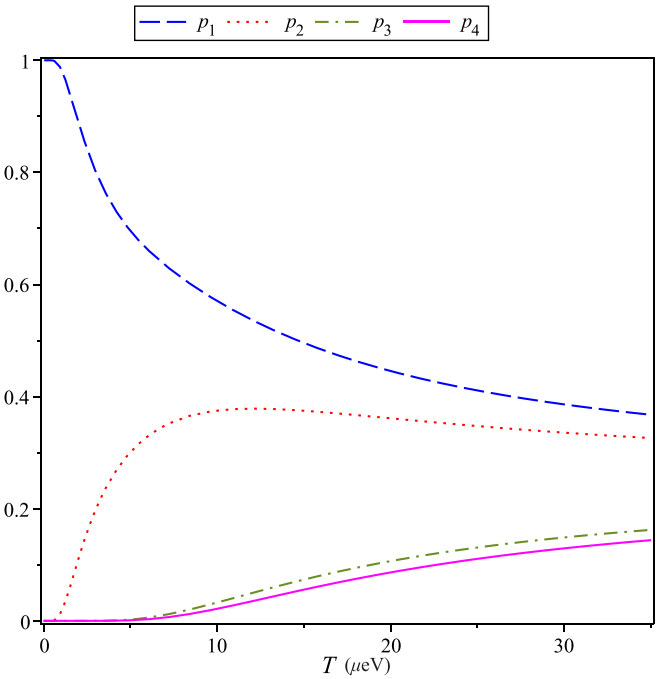

FIG. 11. The occupation probabilities p_n against the temperature T for fixed values: $V = 10\ \mu$eV, $\Delta_1 = 10\ \mu$eV, and $\Delta_2 = 3\ \mu$eV.

ACKNOWLEDGMENTS

This study was financed in part by the Coordenação de Aperfeiçoamento de Pessoal de Nível Superior, Brasil (CAPES), Finance Code 001. M. Rojas acknowledges CNPq Grant No. 432878/2018-1 and C. Filgueiras acknowledges CNPq Grant No. 305077/2018-0. We thank the referees for the valuable suggestions.

APPENDIX A: WORK CURVES FOR DIFFERENT VALUES OF COULOMB COUPLING

In order to achieve an optimized value for the work done by the heat engine, we plot in the Fig. 10 the work done W against the tunneling parameter Δ_2 for some different values of the Coulomb coupling V_c (it could also be Δ_1 because, as we discussed early, the Hamiltonian is symmetric). Thus, we fix $V_h = 10\ \mu$eV and $\Delta_1 = 10\ \mu$eV for the temperatures $T_h = 2\ \mu$eV and $T_c = 1\ \mu$eV, and we can see that the peak of the curve does not shift considerable, so we can approximately estimate the best value for Δ_2, at least for the order of magnitude, that optimize the work done, to know $\Delta_2 \approx 3\ \mu$eV.

Note that, in concordance with Fig. 4, increasing the interaction coupling V_c will increase the work done for a while [dash-dotted green and solid blue (upper) curves], and then it will start to decrease it (dashed red curve). Also we see that for $V_c < V_h$, the work becomes drastically negative [solid magenta (lower) curve], which also agrees with the positive work condition stated in the Fig. 4.

APPENDIX B: PROBABILITIES DISTRIBUTION

In the Fig. 11 we see the occupation probabilities distribution $p_n = \exp(-E_n/kT)/Z$ for the four possible states $|\psi_n\rangle_{n=1..4}$ in terms of the temperature. We see that for $T = 1\ \mu$eV or even $T = 2\ \mu$eV (values used in most of our plots), the second and the third excited states has practically zero probability ($p_3 \approx p_4 \approx 0$) for the system to be found in, this way we can neglect this two most excited states and approximate our system by a two-level one. On the other hand, if we have $T = 10\ \mu$eV or $T = 20\ \mu$eV (values used in Fig. 9), we see that p_3 and p_4 are no longer negligible, thus the two-level approximation is no longer valid.

[1] H. E. D. Scovil and E. O. Schulz-DuBois, Three-Level Masers as Heat Engines, Phys. Rev. Lett. **2**, 262 (1959).

[2] B. D. L. Bernardo, Unraveling the role of coherence in the first law of quantum thermodynamics, Phys. Rev. E **102**, 062152 (2020).

[3] H. T. Quan, Y.-X. Liu, C. P. Sun, and F. Nori, Quantum thermodynamic cycles and quantum heat engines, Phys. Rev. E **76**, 031105 (2007).

[4] F. L. Curzon and B. Ahlborn, Efficiency of a Carnot engine at maximum power output, Am. J. Phys. **43**, 22 (1975).

[5] K. H. Hoffmann, An introduction to endoreversible thermodynamics, Atti Accad. Peloritana Pericolanti Classe Sci. Fis. Mater. Nat. **86**, C1S0801011 (2008).

[6] S. Deffner, Efficiency of harmonic quantum Otto engines at maximal power, Entropy **20**, 875 (2018).

[7] R. Alicki, The quantum open system as a model of the heat engine, J. Phys. A: Math. Gen. **12**, L103 (1979).

[8] O. Abah, J. Roßnagel, G. Jacob, S. Deffner, F. Schmidt-Kaler, K. Singer, and E. Lutz, Single-Ion Heat Engine at Maximum Power, Phys. Rev. Lett. **109**, 203006 (2012).

[9] G. Maslennikov, S. Ding, R. Hablützel, J. Gan, A. Roulet, S. Nimmrichter, J. Dai, V. Scarani, and D. Matsukevich, Quantum absorption refrigerator with trapped ions, Nat. Commun. **10**, 202 (2019).

[10] J. Roßnagel, S. T. Dawkins, K. N. Tolazzi, O. Abah, E. Lutz, F. Schmidt-Kaler, and K. Singer, A single-atom heat engine, Science **352**, 325 (2016).

[11] C. Filgueiras, Quantum heat machines enabled by the electronic effective mass, Results Phys. **15**, 102556 (2019).

[12] Y. Rezek and R. Kosloff, Irreversible performance of a quantum harmonic heat engine, New J. Phys. **8**, 83 (2006).

[13] J. Wang, J. He, and Z. Mao, Performance of a quantum heat engine cycle working with harmonic oscillator systems, Sci. China Ser. G **50**, 163 (2007).

[14] B. Lin and J. Chen, Optimization on the performance of a harmonic quantum Brayton heat engine, J. Appl. Phys. **94**, 6185 (2003).

[15] X. L. Huang, H. Xu, X. Y. Niu, and Y. D. Fu, A special entangled quantum heat engine based on the two-qubit Heisenberg XX model, Phys. Scr. **88**, 065008 (2013).

[16] J.-Z. He, X. He, and J. Zheng, Entangled quantum heat engine based on two-qubit Heisenberg XY model, Chin. Phys. B **21**, 050303 (2012).

[17] H.-P. Peng, M.-F. Fang, and C.-Y. Zhang, Quantum heat engine based on working substance of two particles Heisenberg XXX model with the Dzyaloshinskii-Moriya interaction, Int. J. Theor. Phys. **58**, 1651 (2019).

[18] X. Huang, Q. Sun, D. Guo, and Q. Yu, Quantum Otto heat engine with three-qubit XXZ model as working substance, Physica A **491**, 604 (2018).

[19] Y. Khlifi, A. El Allati, A. Salah, and Y. Hassouni, Quantum heat engine based on spin isotropic Heisenberg models with Dzyaloshinski-Moriya interaction, Int. J. Mod. Phys. B **34**, 2050212 (2020).

[20] M. Josefsson, A. Svilans, A. M. Burke, E. A. Hoffmann, S. Fahlvik, C. Thelander, M. Leijnse, and H. Linke, A quantum-dot heat engine operating close to the thermodynamic efficiency limits, Nat. Nanotechnol. **13**, 920 (2018).

[21] Y. S. Liu, X. F. Yang, X. K. Hong, M. S. Si, F. Chi, and Y. Guo, A high-efficiency double quantum dot heat engine, Appl. Phys. Lett. **103**, 093901 (2013).

[22] T.-H. Kim, K.-S. Cho, E. K. Lee, S. J. Lee, J. Chae, J. W. Kim, D. H. Kim, J.-Y. Kwon, G. Amaratunga, S. Y. Lee, B. L. Choi, Y. Kuk, J. M. Kim, and K. Kim, Full-colour quantum dot displays fabricated by transfer printing, Nat. Photon. **5**, 176 (2011).

[23] X. Dai, Y. Deng, X. Peng, and Y. Jin, Quantum-dot light-emitting diodes for large-area displays: Towards the dawn of commercialization, Adv. Mater. **29**, 1607022 (2017).

[24] O. E. Semonin, J. M. Luther, and M. C. Beard, Quantum dots for next-generation photovoltaics, Mater. Today **15**, 508 (2012).

[25] S. Emin, S. P. Singh, L. Han, N. Satoh, and A. Islam, Colloidal quantum dot solar cells, Solar Energy **85**, 1264 (2011).

[26] S. E. Economou, J. I. Climente, A. Badolato, A. S. Bracker, D. Gammon, and M. F. Doty, Scalable qubit architecture based on holes in quantum dot molecules, Phys. Rev. B **86**, 085319 (2012).

[27] F. Troiani, U. Hohenester, and E. Molinari, Exploiting exciton-exciton interactions in semiconductor quantum dots for quantum-information processing, Phys. Rev. B **62**, R2263(R) (2000).

[28] J. H. Reina, L. Quiroga, and N. F. Johnson, Quantum entanglement and information processing via excitons in optically driven quantum dots, Phys. Rev. A **62**, 012305 (2000).

[29] G. Shinkai, T. Hayashi, T. Ota, and T. Fujisawa, Correlated Coherent Oscillations in Coupled Semiconductor Charge Qubits, Phys. Rev. Lett. **103**, 056802 (2009).

[30] T. Fujisawa, T. Hayashi, and Y. Hirayama, Controlled decoherence of a charge qubit in a double quantum dot, J. Vacuum Sci. Technol. B **22**, 2035 (2004).

[31] P. A. Oliveira and L. Sanz, Bell states and entanglement dynamics on two coupled quantum molecules, Ann. Phys. **356**, 244 (2015).

[32] B. Szafran, Paired electron motion in interacting chains of quantum dots, Phys. Rev. B **101**, 075306 (2020).

[33] F. F. Fanchini, L. K. Castelano, and A. O. Caldeira, Entanglement versus quantum discord in two coupled double quantum dots, New J. Phys. **12**, 073009 (2010).

[34] F. M. Souza, P. A. Oliveira, and L. Sanz, Quantum entanglement driven by electron-vibrational mode coupling, Phys. Rev. A **100**, 042309 (2019).

[35] C. Filgueiras, O. Rojas, and M. Rojas, Thermal entanglement and correlated coherence in two coupled double quantum dots systems, Ann. Phys. **532**, 2000207 (2020).

[36] T. Heinzel, *Mesoscopic Electronics in Solid State Nanostructures* (John Wiley & Sons, New York, 2006).

[37] J. Gorman, D. G. Hasko, and D. A. Williams, Charge-Qubit Operation of an Isolated Double Quantum Dot, Phys. Rev. Lett. **95**, 090502 (2005).

[38] T. Fujisawa, G. Shinkai, T. Hayashi, and T. Ota, Multiple two-qubit operations for a coupled semiconductor charge qubit, Physica E **43**, 730 (2011).

[39] K. D. Petersson, C. G. Smith, D. Anderson, P. Atkinson, G. A. C. Jones, and D. A. Ritchie, Microwave-Driven Transitions in Two Coupled Semiconductor Charge Qubits, Phys. Rev. Lett. **103**, 016805 (2009).

[40] *Thermodynamics in the Quantum Regime* (Springer, Cham, 2018).

[41] R. J. de Assis, J. S. Sales, J. A. R. da Cunha, and N. G. de Almeida, Universal two-level quantum Otto machine under a squeezed reservoir, Phys. Rev. E **102**, 052131 (2020).

[42] S. Chand and A. Biswas, Measurement-induced operation of two-ion quantum heat machines, Phys. Rev. E **95**, 032111 (2017).

[43] D. Gelbwaser-Klimovsky, A. Bylinskii, D. Gangloff, R. Islam, A. Aspuru-Guzik, and V. Vuletic, Single-Atom Heat Machines Enabled by Energy Quantization, Phys. Rev. Lett. **120**, 170601 (2018).